This is a repository copy of *Geometric morphometrics and finite elements analysis:Assessing the functional implications of differences in craniofacial form in the hominin fossil record*.

1

Geometric morphometrics and Finite elements analysis: Assessing the functional implications of differences in craniofacial form in the hominin fossil record

Paul O'Higgins[a], Laura C Fitton[a] and Ricardo Miguel Godinho[a]

5

Paul **O'Higgins (corresponding author)**

a) Hull York Medical School and Department of Archaeology of the University of York

John Hughlings Jackson Building, University of York, Heslington, York YO10 5DD, UK

paul.ohiggins@hyms.ac.uk

10

Laura C. **Fitton**

Hull York Medical School and Department of Archaeology of the University of York

John Hughlings Jackson Building, University of York, Heslington, York YO10 5DD, UK

laura.fitton@hyms.ac.uk

15

Ricardo Miguel **Godinho**[1]

a) Hull York Medical School and Department of Archaeology of the University of York

Academic address: John Hughlings Jackson Building, University of York, Heslington, York

YO10 5DD, UK

b) Interdisciplinary Center for Archaeology and Evolution of Human Behaviour (ICArHEB)

Faculdade das Ciências Humanas e Sociais, Universidade do Algarve, Campus Gambelas,

8005-139, Faro, Portugal

[1] Permanent address: R. Dr. Joaquim Fiadeiro, nº86, Urbanização Tapada do Carapetal, 7200-480 Reguengos de Monsaraz, Portugal

23   ricardomiguelgodinho@gmail.com

24

25

26 **Abstract:**

27 The study of morphological variation in the hominin fossil record has been transformed in
28 recent years by the advent of high resolution 3D imaging combined with improved geometric
29 morphometric (GM) toolkits. In parallel, increasing numbers of studies have applied finite
30 elements analysis (FEA) to the study of skeletal mechanics in fossil and extant hominoid
31 material. While FEA studies of fossils are becoming ever more popular they are constrained
32 by the difficulties of reconstruction and by the uncertainty that inevitably attaches to the
33 estimation of forces and material properties. Adding to these modelling difficulties it is still
34 unclear how FEA analyses should best deal with species variation.

35 Comparative studies of skeletal form and function can be further advanced by applying tools
36 from the GM toolkit to the inputs and outputs of FEA studies. First they facilitate virtual
37 reconstruction of damaged material and can be used to rapidly create 3D models of skeletal
38 structures. Second, GM methods allow variation to be accounted for in FEA by warping
39 models to represent mean and extreme forms of interest. Third, GM methods can be applied
40 to compare FEA outputs – the ways in which skeletal elements deform when loaded. Model
41 comparisons are hampered by differences in material properties, forces and size among
42 models but how deformations from FEA are impacted by these parameters is increasingly
43 well understood, allowing them to be taken into account in comparing FEA outputs.

44 In this paper we review recent advances in the application of GM in relation to FEA studies
45 of craniofacial form in hominins, providing examples from our recent work and a critical
46 appraisal of the state of the art.

47

48 **Keywords:** Form-function; Geometric Morphometrics; Finite Element Analysis; Craniofacial
49 form; Functional performance.

50

51

1. Introduction

52

53 In this paper we consider how the mechanical performance of crania in biting can be
54 estimated and compared among fossils, paying particular attention to how the methods of
55 geometric morphometrics (GM) can facilitate such analyses in combination with
56 biomechanical modelling using finite elements analysis (FEA).

57

58 As with other skeletal elements, crania fulfil mechanical functions, such as housing and
59 protection of organs and provision of a rigid framework for food acquisition and intra-oral
60 processing by the masticatory apparatus (Lieberman, 2011), which comprises jaws, teeth and
61 soft tissues. Thus, much research has focused on the association between cranial form and
62 masticatory function, with the aims of understanding how crania function and how their
63 functional abilities (performances) differ among related species. These differences have
64 underpinned investigations of how skeletal form, function, ecology and behaviour interrelate
65 (Groning, et al., 2011b, Rayfield, 2005, Rayfield, 2007, Rayfield, et al., 2001, Strait, et al.,
66 2010, Strait, et al., 2007, Strait, et al., 2009, Wroe, et al., 2010, Wroe, et al., 2007). In turn,
67 knowledge of these interrelationships has been used to infer ecology and behaviour from
68 skeletal remains of extinct taxa (Attard, et al., 2014, Cox, et al., 2015, Degrange, et al., 2010,
69 Ledogar, et al., 2016, Oldfield, et al., 2012, Rayfield, 2005, Rayfield, et al., 2001, Smith, et
70 al., 2015b, Strait, et al., 2010, Strait, et al., 2009, Wroe, 2008).

71

72 One aspect of performance, bite force, can be directly measured in extant species using force
73 transducers. These have been widely used to measure bite forces in living humans (Braun, et
74 al., 1995, Kikuchi, et al., 1997, Paphangkorakit and Osborn, 1997, Sinn, et al., 1996). In
75 extinct material alternative approaches are required to estimate forces from skeletal evidence,
76 using bony proxies to approximate lever arm lengths and maximum muscle forces based on
77 the relationships between muscle area, intrinsic muscle fibre strength and force production
78 (Gans and de Vree, 1987, Josephson, 1975, Weijs, 1980). Although this provides an estimate
79 of the force produced by muscles it ignores pennation and depends on the validity of the
80 estimates of muscle areas from bony proxies. Muscle force is converted into bite force
81 through the masticatory lever arm system. By measuring in and out-levers of the masticatory
82 system and computing their ratios, it is possible to estimate the mechanical efficiencies of
83 each muscle and to estimate maximal bite forces (Antón, 1990, Demes and Creel, 1988, Eng,

84   et al., 2013, O'Connor, et al., 2005). However, this approach has limitations due to

85   differences between the cross sectional areas estimated via bony proxies and actual

86   physiological muscle cross sectional areas (Eng, et al., 2013, Toro-Ibacache, et al., 2015), and

87   because the lever system of the jaws is often simplified to two dimensions to ease

88   calculations. Bite force can also be predicted using FEA (Wroe, et al., 2010) and by

89   multibody dynamic analysis (MDA) (Bates and Falkingham, 2012, Curtis, et al., 2008, Shi, et

90   al., 2012). MDA can also be used to infer muscle activation patterns given a particular load.

91   These approaches take full account of the three dimensional geometry of the masticatory

92   lever system but retain dependence on the accuracy of input of variables, such as muscle

93   forces, force vector directions and cranial geometry.

94   Bite forces are transmitted to items held between the teeth, and the teeth and cranium

95   experience the bite reaction force. Thus, crania have to be adapted to withstand masticatory

96   forces. In order to assess, explain and compare how the cranium resists occlusal forces,

97   researchers have used several approaches. These include the analysis of simplified

98   biomechanical models of craniofacial anatomy considered in terms of vertical and horizontal

99   column-like structures that buttress the face and channel bite reaction forces (Görke, 1904;

100   Richter, 1920; Endo, 1965; Endo, 1966) and models that consider crania as a cylinder that is

101   twisted during biting (Greaves, 1985; Greaves and Mucci, 1997; Demes, 1987). These

102   models and their underlying assumptions have been tested through the application of strain

103   gauges to directly measure the surface strains experienced during biting (Hylander et al.,

104   1991; Hylander et al., 1992; Ross and Hylander, 1996; Ravosa et al., 2000a; Ravosa et al.,

105   2000b; Ross, 2001; Ross et al., 2011). FEA has also been applied to this task (Ledogar, et al.,

106   2016, Smith, et al., 2015b, Strait, et al., 2010, Strait, et al., 2007, Strait, et al., 2009, Wroe, et

107   al., 2010) but an important issue in such studies is validity of FEA results, do they match

108   reality?

109

110   For this reason validation studies have been carried out to assess the accuracy of prediction of

111   cranial and mandibular deformations, comparing measured with predicted strains (Bright and

112   Groning, 2011, Groning, et al., 2009, Kupczik, et al., 2007, Ross, 2005, Toro-Ibacache, et al.,

113   2016). In so doing, researchers can assess how various input parameters including skeletal

114   geometry, material properties, constraints, applied forces etc. impact FE model results in

115   order to create more realistic models (Ross, 2005, Strait, et al., 2005, Toro-Ibacache, et al.,

116   2016). In general validation studies tell us that accurate strain prediction in any one specimen

117   is difficult and requires careful adjustment of model parameters to achieve valid results.

118

The accuracy of predictions achieved by FEA is, however, entirely dependent on these input parameters, so, acknowledging modelling limitations, researchers have sought to understand the impact of variations and simplifications in FE modelling. This has led to sensitivity studies in which the impact on predicted deformations of varying specific parameters is assessed. Such parameters include the muscle force magnitudes, directions and activation patterns (Cox, et al., 2011, Fitton, et al., 2012, Groning, et al., 2012, Ross, 2005, Sellers and Crompton, 2004), variations in material properties (Cox, et al., 2011, Groning, et al., 2012, Kupczik, et al., 2007, Reed, et al., 2011, Strait, et al., 2005, Toro-Ibacache, et al., 2016), modelling cranial sutures (Kupczik, et al., 2007, Reed, et al., 2011, Wang, et al., 2010), simplifications in model geometry (Fitton, et al., 2015, Toro-Ibacache, et al., 2016), modelling the periodontal ligament (Groning, et al., 2012, Holland, 2013, McCormack, et al., 2014, Wood, et al., 2011), impact of variations in modelling of trabecular bone (Parr, et al., 2013) and model constraints (Cox, et al., 2011). Validation and sensitivity studies have shown that modelling variations that affect model stiffness (e.g. bone thicknesses, how cancellous bone is represented, material properties, etc.) or total applied force tend to lead to differences in magnitude rather than mode of deformation, while variations in relative muscle activations, muscle vectors and constraints tend to impact mode of deformation, how the cranium deforms (Fitton, et al., 2015, Godinho, et al., 2017, Parr, et al., 2012, Toro-Ibacache, et al., 2016).

138

Researchers have tried to predict how fossil hominin crania resist biting. Such analyses have until recently relied on geometrical simplifications of crania (Demes, 1987, Rak, 1983, Rak, 1986, Trinkaus, 1987). More recently, FEA has been used to more fully model fossil hominin masticatory biomechanics with the aim of improving prediction of the stresses and strains experienced by fossil crania as they deform during biting (Ledogar, et al., 2016, Smith, et al., 2015b, Strait, et al., 2010, Strait, et al., 2009, Wroe, et al., 2010). Sensitivity studies are of particular relevance here as validation is not possible for fossils. FEA applied to fossils has become popular (Cox, et al., 2011, Cox, et al., 2012, Rayfield, 2007, Strait, et al., 2013, Strait, et al., 2010, Strait, et al., 2007, Strait, et al., 2009, Wroe, et al., 2010, Wroe, et al., 2007) and models are frequently based on medical CT scans. However, another challenge of fossils arises because they are often fragmented and invaded by sedimentary matrix that, due to mineralization processes, is undistinguishable, or at least very difficult to distinguish, from bone in scans. This often precludes, for example, segmentation of sedimentary matrix from

152 bone and does not allow fossils to be modelled reliably in terms of their full anatomical

153 complexity. Indeed, given the multiscale organisation of bone, teeth and soft tissues, it is not

154 within the reach of present technology to produce an accurately realistic model. Moreover,

155 increasing model complexity demands higher computational power for solution (Groning, et

156 al., 2012).

157

158 Model simplification in geometry is therefore useful and necessary to overcome these

159 limitations (Fitton, et al., 2015). Assessment of the impact of simplifications typically relies

160 on comparison of variables of interest in subsequent FEA. Thus, researchers commonly focus

161 on stress/strain magnitudes and directions and compare how different modelling decisions

162 impact on those variables (Groning, et al., 2012, Reed, et al., 2011, Strait, et al., 2005,

163 Szwedowski, et al., 2011, Wood, et al., 2011), although bite force has also been used to

164 assess model sensitivity (Fitton, et al., 2012, Sellers and Crompton, 2004). Beyond this, the

165 methods of geometric morphometrics have recently been applied to this task; to compare the

166 deformations of variant models and estimate the impact of such simplifications on results

167 (Fitton, et al., 2015, Fitton, et al., 2012, Godinho, et al., 2017, Toro-Ibacache, et al., 2016).

168

169 The application of GM methods to FEA output is discussed below in more detail, as it is

170 used for the reconstruction of fossils for FEA and in the creation of models of interesting real

171 and hypothetical forms.

172

173 ## 2. How GM can help in reconstruction

174 Once the segmentation process is finished, reconstruction of missing anatomical regions

175 begins.   This   process   usually   combines   imaging   software   (e.g.

176 Avizo/Amira/Mimics/Geomagic) and GM to approximately restore the original geometry of

177 an incomplete or distorted specimen (Weber, 2015, Weber and Bookstein, 2011). In

178 specimens that preserve one side intact, the most straightforward approach is to use bilateral

179 symmetry (Gunz, et al., 2009). In such cases it is possible to reflect the preserved regions

180 onto the incomplete side and use them to replace the missing areas (Gunz, et al., 2009).

181 However, no skeletal structures are completely symmetric and they present different

182 magnitudes of asymmetry (Quinto-Sánchez, et al., 2015). Thus, reflected regions will not

183 perfectly fit the remaining preserved anatomy. To overcome this mismatch, and account for

184 asymmetry, it is possible to use the thin plate spline (TPS) function to warp the reflected

185 structure onto the remaining preserved anatomy (Gunz, et al., 2009). Even though this is a

186 desirable approach, fossils often lack preserved structures on both sides or along the midline,

187 thus precluding reflection. In these cases reference based reconstruction (Gunz, et al., 2004,

188 Gunz, et al., 2009) should be used. The choice of reference specimen should be considered

189 carefully so as to not bias the reconstruction and it has been suggested that references should

190 be species specific (Gunz, et al., 2009, Senck, et al., 2015, Zollikofer and Ponce de León,

191 2005). Such reconstructions may be statistical or geometric (Gunz, et al., 2004, Gunz, et al.,

192 2009, Neeser, et al., 2009). Statistical reconstruction uses covariances among landmarks in a

193 given sample to predict the location of missing landmarks via multivariate regression (Gunz,

194 et al., 2009, Neeser, et al., 2009). Geometric reconstruction uses the TPS function to estimate

195 the position of the missing landmarks based on known ones (Gunz, et al., 2004, Gunz, et al.,

196 2009). The latter has the advantage of requiring one single specimen, which may be a

197 particular individual or a mean specimen calculated from a given sample using GM (Gunz, et

198 al., 2009) but omits information on intra specific covariations. However, Senck and

199 Coquerelle (2015) show that using mean specimens yields good results when reconstructing

200 large portions of incomplete specimens. Further where sample sizes are limited to one or a

201 few specimens, as with fossils, TPS based warping can be applied, whereas statistical

202 approaches cannot.

203

204 **3. How GM can generate interesting hypothetical forms**

205 Transforming an existing model into a target specimen is of significant value in allowing us

206 to visualise the results of GM analyses. To that end an original specimen may be landmarked

207 densely and then warped into a target that was landmarked similarly (O'Higgins, et al., 2011,

208 Stayton, 2009). Models that represent extremes of morphological variation within a taxon

209 may be created applying a similar approach. Such models can readily be used to simulate

210 mechanical loading and examine the impact of intra-specific morphological variance on

211 mechanical function (Smith, et al., 2015a). One major obstacle to using such an approach is

212 that accurate warping of one specimen into another requires many landmarks and

213 semilandmarks and even then, internal structures such as tooth roots, sinuses and cancellous

214 bone are unlikely to be warped to the form they would have in the target specimen. This is

215 because such internal architecture is very finely detailed and sinuses and cancellous bone

216 architecture are, to great extent, the result of adaptation in the specific individual to habitual

217 loading, this is not accounted for by warping alone. Any errors in warping will therefore

likely impact the resulting deformations of the FE model. An alternative is to warp 'solid' models, ones in which all that is represented is the geometry of the cranial surfaces with the spaces in between infilled with homogenous material. Cancellous bone and sinuses are filled and teeth are not represented as distinct structures, but merely as material with the properties of bone, and with roots merged with the surrounding bone. This is a drastic manoeuvre and a gross simplification. As such, the question arises as to what solid simplified models can tell us?

Parr et al. (2012) examined the impact of infilling mandibular cavities on the deformations (bending displacements and strain magnitudes frequency) experienced by the mandible of a varanoid lizard during simulated loading. They show that models with infilled cavities deform less than, but generally similarly to, models with preserved cavities. Likewise, Fitton et al. (2015) investigated the effects of simplifying details of internal anatomy (presence/absence of the maxillary sinus) and material properties of teeth in a *Macaca fascicularis* cranium, concluding that it does not impact significantly on large scale deformations but it does have localized effects in strain distributions. Toro-Ibacache (2016) addressed the impact of segmentation protocols and of simplifying material properties of a cadaveric human cranium. They concluded that segmentation protocols can have a significant impact on large scale deformations but that simplifying material properties (differentiating trabecular bone from cortical bone vs not differentiating between the two) had little impact on mode of deformation. Thus, if constraints and loads are held constant, solid models behave similarly to much more detailed ones. The key difference emerging from these studies is that the solid models deform less, and so absolute magnitudes of deformation (measured as strains or in terms of changes in size and shape; see below) are not accurately predicted while the mode of deformation (how it deforms) is more consistent. This leads to the realisation that solid models are useful in studies where absolute magnitudes of strains are of no interest but rather, the focus is on mode, how a cranium deforms.

These findings open up the possibility of carrying out many interesting 'virtual experiments' by warping or modifying skeletal anatomy to predict the functional role of particular features (O'Higgins, et al., 2011). Strait et al. (2007) applied this virtual experiment approach to infer the relevance of thick palates in Austalopiths by experimentally thickening the hard palate of a *Macaca fascicularis* and measure resulting strains. Fitton et al. (2009) reconstructed a specimen of *Austrolopithecus africanus* (STS 5) and warped the zygomatic region to that of a

252 *Paranthropus boisei* (OH 5) while maintaining the remaining anatomy constant. In both
253 cases, the impact of such modifications was assessed in terms of their impact on stresses and
254 strains in the face.

255

256 **4. How GM can be used to compare FEA results**

257 While stresses and strains from FEA are informative with regard to how skeletal structures
258 bear loads and where they are likely to fail at a localized level (elements or nodes of
259 elements) they do not allow ready assessment of how the model deforms as a whole, for
260 instance, how it bends, twists and undergoes other changes in size and shape. Rather, such
261 modes have to be inferred from strain contour maps based on expertise and knowledge.
262 GM, on the other hand, uses configurations of landmark coordinates and multivariate
263 statistics to assess how specimens differ in form, thereby quantifying morphological
264 differences in size and shape. Thus, it has been proposed that GM can be used to measure and
265 describe global deformations (defined here as changes in size and shape) of models under
266 loading (O'Higgins, et al., 2011, O'Higgins, et al., 2012). This approach differs from GM
267 shape analyses in that size is also simultaneously considered, because loadings change the
268 shape and the size of objects. The basis and application of this approach is described more
269 fully in section 5.3.

270

271 **5. Example Studies**

272 To illustrate how the approaches described above are applied in practice, example studies are
273 presented and reviewed, below.

274

275 **5.1 Reconstruction of crania**

276 We illustrate the application of GM to reconstruction using a CT scan of the cranium of
277 Kabwe 1, which is remarkably well preserved but still presents missing and damaged
278 anatomy due to taphonomic and pathological processes (Schwartz and Tattersall, 2003).
279 Missing anatomical regions include a large portion of the right side of the cranial vault and
280 base (affecting parts of the right temporal, parietal, zygomatic and occipital bone), a small
281 region of the alveolus of the maxilla, teeth and small portions of the orbital cavities (Figure
282 1A). The reconstruction was based on a CT scan (courtesy of Robert Kruszynski, Natural

283 History Museum, London) performed using a Siemens Somatom Plus 4 CT scanner, with

284 voxel size of 0.47 x 0.47 x 0.50 mm and 140 kVp. Reconstruction started with the

285 segmentation of the existing anatomy from the volume. Reconstruction of the left side of the

286 vault followed, and this was later used to restore the large region missing from the right side

287 of the cranium. Lastly, all remaining missing anatomical regions were reconstructed.

288 Segmentation was performed in Avizo 7.0 (Visualization Sciences Group Inc.) and used a

289 variety of approaches. The initial segmentation applied a half maximum height value

290 (HMHV; Spoor et al., 1993) to the whole volume to threshold segment it. Regional

291 thresholds were subsequently calculated and applied to specific anatomical regions as a

292 second step because the HMHV did not segment thin bones. Manual segmentation was also

293 applied for fine details of thin bones that were not picked up by the two previous approaches.

294 Because teeth present clearly different grey values specific thresholds were calculated and

295 applied so as to not overestimate their dimensions. Last, existing sedimentary matrix was

296 removed manually.

297

298 Once the segmentation of existing structures was complete, the large missing region of the

299 right half of the cranium was restored by reflecting the existing contralateral half and fitting

300 (warping) it to the existing structures. This last step used the TPS function and is necessary

301 because crania are not absolutely symmetric. This warping is achieved by placing matching

302 landmarks on the damaged region and reflected fragment and then deforming (warping) the

303 fragment to the cranium using the 'Bookstein' warping function. This resulted in an almost

304 perfect fit between the restored and preserved anatomy, requiring only minimal manual

305 editing. Restoration of the damaged alveolar process of the right hemi-maxilla was also

306 achieved by reflecting the preserved left region. Existing gaps (such as the one present in the

307 orbital surfaces of the maxilla and ethmoid, internal nasal walls, maxilla, occipital bone, left

308 temporal bone, ethmoid bone and vomer) were restored using a combination of manual

309 editing and the software Geomagic Studio 2011 (courtesy of DR W. Sellers, University of

310 Manchester) to interpolate between existing bone edges. The missing posterior region of the

311 occipital bone was reconstructed using the occipital of a modern human cranium, which was

312 manually edited using Geomagic to adjust its morphology. Teeth were preferentially restored

313 by reflecting existing antimeres. When this was not possible portions of teeth from a modern

314 human were used to reconstruct incomplete teeth (final result of reconstruction in Figure 1B).

315

316

317   Figure 1

318

319

320   **5.2 Hypothetical forms**

321   FEA may be applied to any model, whether it represents a real specimen or not. For instance

322   a prior GM analysis may have established the mean form and limits of variation of a

323   landmark configuration taken on a sample of crania. Rather than be interested in how any

324   particular specimens perform, we may be interested in the range of performances represented

325   by the sample. Earlier we noted that solid models, in which internal detail is grossly

326   simplified and filled, provide a reasonable basis for experimental manipulation of FE models

327   to assess specific questions such as the effects of varying palatal thickness or maxillary

328   morphology. This same principle can be extended to whole landmark configurations such as

329   those representing the limits of variation of a sample. By using triplets of thin plate splines to

330   warp whole crania between the mean and these limits of variation hypothetical crania can be

331   created. They do not represent real crania but rather a statistical result from prior

332   morphometric analyses, in this case limits of variation but also, feasibly, through regression

333   or partial least squares (PLS), they could represent forms at the limits of cranial covariation

334   with some interesting ecological or functional variables (e.g. climatic or dietary data,

335   measured bite forces etc.). FEA is then carried out on these hypothetical forms to see how the

336   modes of variation of cranial form identified in the analysis impact performance when the

337   cranium is loaded.

338

339   This warping approach is illustrated here using a simple example; the Kabwe 1 cranium

340   warped into a mean Neanderthal (model 2) using thin plate splines based on classical and

341   sliding semi-landmarks. Classical landmarks (Figure 2, red spheres) of the mean Neanderthal

342   were calculated from 4 Neanderthal crania (Gibraltar 1, Guattari, La Chapelle-aux-Saints, La

343   Ferrassie). The sliding semi-landmarks on the maxilla and brow-ridge (yellow spheres) were

344   calculated from the 4 specimens and the sliding semi-landmarks of the vault and zygoma

345   (light blue spheres) were calculated from the 2 crania in which these structures are almost

346   completely preserved (Guattari and La Ferrassie). In Figure 2, the original model of Kabwe is

347   shown on the left (Figure 2A) and the warped 'mean Neanderthal' on the right (Figure 2B). It

348   is clear that a visually satisfactory result is obtained but of course internal architecture (tooth

349 roots, cortical thicknesses, cavities, sinuses and cancellous bone) will also be warped, not
350 necessarily in such a way that they reasonably represent the average form in Neanderthals.
351 However, by using 'solid' models as described above such errors are avoided. The FEA in
352 such a circumstance does not aim to predict and compare actual deformations but rather it
353 provides an answer to a different type of question: how do the differences in external form
354 between these models impact mode and magnitude of deformation?

355 This approach is more limited than we may wish but it is useful in many contexts, for
356 instance in considering how facial retraction vs projection, or brachycephaly vs
357 dolichocephaly, or the mode of form variation predicted by e.g. climate or diet etc. impact on
358 model performance. These are more general questions whose answer does not rest on study
359 of single specimens, but rather on consideration of general modes of variation and their
360 general effects.

361
362

363 Figure 2

364
365

366 **5.3 Application of GM methods to the comparison of FEA results**

367 As noted earlier a third way in which GM methods complement FEA is through comparison
368 of deformations that occur due to loading (O'Higgins, et al., 2011, O'Higgins, et al., 2012).
369 This approach has been applied in several studies (Cox, et al., 2011, Fitton, et al., 2015,
370 Groning, et al., 2012, Groning, et al., 2011a, Holland, 2013, Prôa, 2013, Toro-Ibacache, et al.,
371 2016). Such analyses of deformation rely on assessment of changes in model size and shape,
372 rather than of shape alone as is common in GM studies of organismal variation. This is
373 because as a model is loaded it changes in both size and shape, and it makes no sense to focus
374 on one aspect alone (shape or size). In consequence size and shape are analysed jointly, using
375 rescaled shape coordinates from GPA. The resulting size and shape distances between
376 unloaded and loaded forms describe the magnitudes of deformation and the direction of the
377 vector connecting unloaded and loaded forms in the size and shape space describes the mode
378 of deformation. These vectors can be compared among different load cases applied to the
379 same model or among different models by ignoring the differences in size and shape among
380 unloaded forms and focussing in the vectors connecting unloaded and loaded forms.

13

381   We illustrate the application of this approach by summarizing a study (Godinho, et al., 2017,

382   Toro-Ibacache, et al., 2016) that examines the impact of simplifications of a cadaveric *Homo*

383   *sapiens* cranium on the resulting modes of deformation predicted by FEA. Specifically, it

384   assesses the impact of simplifications among a three materials model (cortical bone,

385   cancellous bone and teeth; model 3), a two materials (cortical bone and teeth; model 2) and a

386   one material model (everything with material properties of cortical bone; model 1). Thus

387   model 1 is a simple 'solid' model (see above) and model 3 is a much more anatomically

388   accurate model. The models are loaded to simulate a bite on the first molar, although the

389   applied forces are not physiological, rather they replicate the loading of an accompanying

390   validation study to facilitate comparison with that in ongoing work.

391   The results in terms of strain contour plots (not shown), suggest that variations among models

392   generally impact on magnitudes of strains but not so much on the distribution of regions of

393   high and low strain throughout the model. The GM analysis of deformations complements

394   these findings. Size and shape distances are calculated by multiplying the shape coordinates

395   (from GPA) of each specimen by that specimen's original centroid size. This results in the

396   specimens being represented by points in a (size and shape) space that can be thought of as

397   the space of GPA aligned coordinates (Slice 2001), an approximation of Kendall's shape

398   space, with size as an additional dimension. The vector of centroid size (the additional

399   dimension) at any point on the manifold can be visualised as passing radially from the

400   centroid of the manifold of this space (zero size), through the manifold (centroid size = 1) and

401   beyond to infinity (infinite size). When centroid size is 1, the objects lie on the manifold of

402   the space of GPA aligned coordinates (Figure 3). The resulting space differs from the classic

403   size and shape space (Dryden and Mardia, 1998) that results from translating and rotating, but

404   not scaling landmark configurations. In particular, the rotations of configurations with respect

405   to each other differ because size influences rotation. In consequence the estimates of mean

406   size and shape (the size and shape variables; translated and rotated coordinates) obtained by

407   these two approaches, the resulting covariance matrix, and so PCA, also differ. However in

408   the application to FEA, where deformations are extremely small, the resulting size and shape

409   differences are negligible. Either space could be used, with almost no difference in results,

410   but the approach we adopt is useful in understanding how shape analysis and size and shape

411   analysis are related (Figure 3). Thus, simply making the model stiffer or less stiff (material

412   properties) or applying the same force vectors but varying their magnitudes results in greater

413   or less deformation; the vectors connecting unloaded and loaded models simply scale directly

414   with force or inversely with Young's modulus (a measure of stiffness). Deformations (size

415 and shape distances) also scale inversely with model centroid size if loads, geometry and
416 material properties are held constant. In contrast Procrustes distances scale inversely with the
417 square of centroid size. Figure 3 illustrates these scaling relationships with centroid size.
418 Thus if we take the shape of the black point (a; on the GPA hemisphere, centroid size =1;
419 Fig. 3) to be the unloaded form and the grey point (b) as the shape of the loaded form, the
420 distance between them represents the deformation in shape and approximates Procrustes
421 distance when variations are small. If size also differs due to loading, then the loaded form
422 does not lie on the hemisphere but is above (grey point, c) or below it depending on if it
423 increased or decreased in centroid size. The distance (a-c) between loaded and unloaded
424 forms is the size and shape distance and is a measure of deformation (change in size and
425 shape with loading).

426

427 If the same forces and same material properties apply but the unloaded form is larger (black
428 point, d, on the outer semicircle representing the GPA hemisphere with centroid size >1 in
429 Fig 3) the resulting deformation in size and shape is less (distance d-f; which in this diagram
430 is shown larger than in reality to facilitate visualisation). The physics dictate that the size and
431 shape distances (deformations) between unloaded and loaded objects scale inversely with
432 centroid sizes of the unloaded objects; bigger forms deform less under the same load.
433 However, shape change due to loading (Procrustes distance as opposed to size and shape
434 distance) scales inversely with the *square* of the centroid size of the unloaded object. Thus,
435 scaling the unloaded large object, d, to centroid size 1, results in it overlying point a, the
436 unloaded object with centroid size 1 (these are identical in shape but differ only in size).
437 Scaling the loaded large object, f, to centroid size 1 projects it along a radius (dashed line in
438 Fig. 3) through point e to an intersection, g, with the arc of the GPA hemisphere. As a result
439 of this scaling, the ratio of Procrustes distances (a-b)/(a–g) is the inverse of the ratio of the
440 squares of centroid sizes of the unloaded forms, a and d.

441

442 These scaling ratios are important because they allow us to account (at least approximately)
443 for differences in size when comparing deformations predicted by FEA among similar objects
444 using geometric morphometric methods. Such scaling is inevitably an approximation unless
445 the objects whose deformations are being compared are the same shape, differing only in
446 size. As shapes become more different, it makes less sense to compare deformations and the
447 degree of approximation in scaling increases.

448

449   Figure 3

450

451

452   Principal components analysis using the covariance matrix among size and shape variables

453   can be used to visualise and compare deformations. Figure 4 presents the first two principal

454   components from the sensitivity study we conducted on a *Homo sapien*s of model

455   simplification with regard to segmentation and allocation of material properties. These

456   account for some 99% of the total variance and so fairly represent the results. Included in the

457   analysis are the unloaded model and the three variants of model segmentation (model 1,

458   whole model as cortical bone = 17 GPa; model 2, bone = 17 GPa and teeth = 50 GPa; model

459   3, cortical bone = 17GPa, cancellous bone = 56 MPa, teeth = 50 GPa; all materials allocated a

460   Poisson's ratio of 0.3) after loading in a simulated first molar bite. Model 3 is also loaded in a

461   simulated incisor bite. This allows the effects of simplification to be compared against the

462   effect of varying bite point. The molar bites cluster away from the incisor bite, indicating

463   they are more similar in mode of deformation. The modes of variation are represented by the

464   vectors connecting unloaded and loaded models. They are visualised by the inset warped

465   surface models and transformation grids, computed using thin plate splines and magnified

466   500 times to facilitate interpretation. Models 2 and 1 overlie each other and so are represented

467   by a single point. This implies that representing dental roots as cortical bone has little effect.

468   Modes of deformation differ greatly between incisor and molar bites and consist mainly of

469   upwards deflection of the anterior maxilla in the former and of the lateral maxilla in the latter.

470   With regard to the molar bites, simplification has its greatest impact when cancellous bone is

471   allocated the material properties of cortical, effectively making a 'solid' model. The effect is

472   to reduce the degree of deformation as is reflected in the shorter vector connecting models 1

473   and 2 with the unloaded than that connecting model 3. Similarly the degree of deformation

474   evident in the inset warpings is reduced. There is a difference in mode of deformation as

475   evidenced by the angle between these vectors but the difference in mode is less obvious in

476   comparing the inset warping for models 2 and 3 with that for model 1.

477   The impact of simplification on mode of deformation is small compared to the large

478   difference between molar and incisor bites.

479

480

481   Figure 4

482

483

484   This simple analysis can be extended to more complex and interesting questions concerning

485   multiple variants of models and to the comparison of deformations among models (O'Higgins

486   and Milne, 2013) by focusing on differences among vectors of deformation rather than

487   differences among unloaded forms. This application of GM is particular useful in relation to

488   FEA sensitivity studies providing an easily visible and quantifiable approach to the

489   assessment of model "error" and sensitivity. Comparisons can be made within and between

490   models to assess whether differences in performance due to modelling assumptions are

491   drowning out any meaningful biological signals.

492

493   **6. Discussion**

494   The last three decades have seen an explosion of advances in techniques pertinent to the

495   study of skeletal change through time. Morphometrics underwent a revolution (Adams, et al.,

496   2004, Rohlf and Marcus, 1993) beginning in the late 1970's (Bookstein, 1978) and gathering

497   pace through the next three decades. This, in common with the tools for high resolution

498   imaging, visualisation and manipulation of images, took great advantage of the advances in

499   computing that occurred over the same period. These same advances in computational power

500   led to the development of increasingly sophisticated software tools for FEA, to simulate and

501   predict the effects of loadings on structures.

502

503   All of these tools are in common use today in the field of Archaeology, in particular they

504   have been driven by work on fossil material, but increasingly they are applied to more recent

505   skeletal finds, archaeobotany (García-Granero, et al., 2016, Ros, et al., 2014), zooarchaeology

506   (Cucchi, et al., 2011, Evin, et al., 2013, Owen, et al., 2014) and to material culture such as

507   ancient architecture (Levy and Dawson, 2009), stone tools (Buchanan and Collard, 2010,

508   Buchanan, et al., 2011, Okumura and Araujo, 2014), and pottery (Hein, et al., 2008,

509   Kilikoglou and Vekinis, 2002, Wilczek, et al., 2014). As these tools have become more

510   commonly applied, useful ways of combining them have come to the fore. Thus, GM

511   methods combined with tools for imaging and image manipulation can play an important role

512   in the reconstruction of skeletal material, as illustrated by the first example we present in this

513   paper.

17

514

515 Reconstruction provides data for morphometric analyses and GM has proven powerful in this

516 domain. Beyond the fact that these methods provide approaches that are statistically robust

517 and well understood, GM's great advantage for many workers lies in the ability to visualise

518 the results of statistical analyses as warpings of the mean form. These visualisations close the

519 loop between measurement, statistics and interpretation of results in terms of changes in size

520 and shape. They also can be used to produce 3D models of the results of statistical analyses

521 such as mean forms or forms representing extremes of variation or extremes of interesting

522 modes of variation, such as the limits of regressions of form on ecological, behavioural and

523 functional data. In turn, such forms are potentially interesting targets for FEA. For instance,

524 the results of a study of how cranial form covaries with the toughness of diet might be

525 actualised as a pair of 3D surfaces representing crania at the limits of the regression; those

526 suited to tough and those suited to less tough diets. These can be submitted to FEA to explore

527 how each responds to loading and, in this way, link modes of morphological variation to load

528 resistance. This kind of analysis provides a very direct way of exploring how form and

529 function interact.

530

531 These kinds of studies depend critically on the validity of FEA modelling and on how

532 sensitive such modelling is to errors in model building and loading. Validity is assessed by

533 comparing predicted strains with directly measured, real strains. Sensitivity, on the other

534 hand is assessed by varying model parameters to replicate likely errors and comparing results

535 among (often many) variant models as in the example we provide earlier. In this endeavour,

536 GM has been usefully combined with FEA.

537

538 Size and shape analysis allows ready understanding of the effects of different model building

539 decisions in terms of how the models deform and how they differ in deformation. It leads to

540 statements about changes in form such as how a skull twists or bends under loading. If,

541 instead of landmarks the coordinates of all nodes of the finite element mesh are submitted to

542 analysis, strains can be computed from the coordinates of the unloaded and loaded meshes.

543 On the other hand the concentrations of stresses or strains in localised regions are useful

544 predictors of failure and while the overall distribution of strains can be used to infer global

545 modes of deformation this requires simultaneous interpretation of one contour map for each

546 principal strain (2 in 2D analyses and 3 in 3D). Thus the approaches can be considered

547 complementary. GM analyses inform with regard to how loading deforms an object, in terms

548 of changes in size and shape. On the other hand, stresses and strains inform with regard to the

549 likelihood of failure in particular anatomical regions and how distributions of high and low

550 strains may eventually relate to (re)modelling fields. Each can be used to infer the other, thus

551 GM analyses that use the coordinates of the nodes of an FE mesh result in visualisations of

552 deformations of that mesh and strains can be computed and displayed in these meshes, while

553 strains can be used to infer global degrees and modes of deformation. It should be noted that

554 the metric of the GM analysis, the Procrustes size and shape distance relates to changes in

555 size and shape, not the risk of failure. It differs from metrics derived from strains. These

556 describe different aspects of deformation that are complementary, but not coincident, in

557 interpreting FEA results.

558

559 Beyond sensitivity analyses, GM methods have been extended to the task of comparing

560 deformations among different specimens modelled and loaded in equivalent ways (Milne and

561 O'Higgins, 2012, O'Higgins and Milne, 2013). In this case the analysis focuses on differences

562 in vectors of deformation rather than the differences between unloaded forms. This is

563 achieved by computing deformations as differences between registered loaded and unloaded

564 forms. They can be visualised by adding these vectors to a convenient unloaded form such as

565 the mean of all unloaded specimens. Beyond comparisons of deformation, it is also possible

566 to use GM approaches to assess the association between deformation under loading and other

567 interesting factors such as skeletal form or ecological variables through regression of PLS

568 analyses. This has not yet been much exploited in the literature but is likely to increasingly be

569 taken up as a useful approach to the interpretation of the biological significance of differences

570 in modes and magnitudes of variation. Differences among models in size, applied forces and

571 material properties can be taken into account by 'correcting' the magnitudes of deformations

572 according to the known scaling relationships described above.

573

574 The application of GM methods in conjunction with FEA is as yet in its infancy. There are

575 clear roles for GM methods in reconstruction, the production of models with modified

576 geometry to explore how form and function interact and in comparing the results of FEAs

577 among models and load cases. Each of these approaches has potential benefits and pitfalls

578 and, in time, with increasing numbers of studies applying these methods we will better

579 understand where they are applicable and where not. At present these combined GM/FEA

580 approaches are still fairly novel and some years of methodological development can be

581 anticipated.

582

Acknowledgements

589

590   **References**

591

592   Adams, D.C., Rohlf, F.J., Slice, D.E., 2004. Geometric morphometrics: ten years of progress

593   following the 'revolution', Italian Journal of Zoology 71, 5-16.

594   Antón, S.C., 1990. Neandertals and the anterior dental loading hypothesis: a biomechanical

595   evaluation of bite force production, Kroeber Anthropological Society Papers 71-72, 67-76.

596   Attard, M.R.G., Parr, W.C.H., Wilson, L.A.B., Archer, M., Hand, S.J., Rogers, T.L., Wroe,

597   S., 2014. Virtual Reconstruction and Prey Size Preference in the Mid Cenozoic Thylacinid,

598   *Nimbacinus dicksoni* (Thylacinidae, Marsupialia), Plos One 9, e93088.

599   Bates, K.T., Falkingham, P.L., 2012. Estimating maximum bite performance in

600   Tyrannosaurus rex using multi-body dynamics, Biol Letters 8, 660-664.

601   Bookstein, F., 1978. The Measurement of Biological Shape and Shape Change, Springer,

602   Berlin.

603   Braun, S., Bantleon, H.-P., Hnat, W.P., Freudenthaler, J.W., Marcotte, M.R., Johnson, B.E.,

604   1995. A study of bite force, part 1: Relationship to various physical characteristics, The

605   Angle Orthodontist 65, 367-372.

606   Bright, J.A., Groning, F., 2011. Strain Accommodation in the Zygomatic Arch of the Pig: A

607   Validation Study Using Digital Speckle Pattern Interferometry and Finite Element Analysis,

608   Journal of Morphology 272, 1388-1398.

609   Buchanan, B., Collard, M., 2010. A geometric morphometrics-based assessment of blade

610   shape differences among Paleoindian projectile point types from western North America, J

611   Archaeol Sci 37, 350-359.

612   Buchanan, B., Collard, M., Hamilton, M.J., O'Brien, M.J., 2011. Points and prey: a
613   quantitative test of the hypothesis that prey size influences early Paleoindian projectile point
614   form, J Archaeol Sci 38, 852-864.

615   Cox, P.G., Fagan, M.J., Rayfield, E.J., Jeffery, N., 2011. Finite element modelling of squirrel,
616   guinea pig and rat skulls: using geometric morphometrics to assess sensitivity, J Anat 219,
617   696-709.

618   Cox, P.G., Rayfield, E.J., Fagan, M.J., Herrel, A., Pataky, T.C., Jeffery, N., 2012. Functional
619   Evolution of the Feeding System in Rodents, Plos One 7.

620   Cox, P.G., Rinderknecht, A., Blanco, R.E., 2015. Predicting bite force and cranial
621   biomechanics in the largest fossil rodent using finite element analysis, J Anat 226, 215-223.

622   Cucchi, T., Hulme-Beaman, A., Yuan, J., Dobney, K., 2011. Early Neolithic pig
623   domestication at Jiahu, Henan Province, China: clues from molar shape analyses using
624   geometric morphometric approaches, J Archaeol Sci 38, 11-22.

625   Curtis, N., Kupczik, K., O'Higgins, P., Moazen, M., Fagan, M., 2008. Predicting skull
626   loading: Applying multibody dynamics analysis to a macaque skull, Anat Rec 291, 491-501.

627   Degrange, F.J., Tambussi, C.P., Moreno, K., Witmer, L.M., Wroe, S., 2010. Mechanical
628   Analysis of Feeding Behavior in the Extinct "Terror Bird" *Andalgalornis steulleti*
629   (Gruiformes: Phorusrhacidae), Plos One 5, e11856.

630   Demes, B., 1987. Another Look at an Old Face - Biomechanics of the Neandertal Facial
631   Skeleton Reconsidered, J Hum Evol 16, 297-303.

632   Demes, B., Creel, N., 1988. Bite Force, Diet, and Cranial Morphology of Fossil Hominids, J
633   Hum Evol 17, 657-670.

634   Dryden, I.L., Mardia, K.V., 1998. Statistical Shape Analysis, Wiley-Blackwell.

635   Eng, C.M., Lieberman, D.E., Zink, K.D., Peters, M.A., 2013. Bite force and occlusal stress
636   production in hominin evolution, Am J Phys Anthropol 151, 544-557.

637   Evin, A., Cucchi, T., Cardini, A., Strand Vidarsdottir, U., Larson, G., Dobney, K., 2013. The
638   long and winding road: identifying pig domestication through molar size and shape, J
639   Archaeol Sci 40, 735-743.

640   Fitton, L., Groening, F., Cobb, S., Fagan, M., O'Higgins, P., 2009. Biomechanical
641   Significance of Morphological Variation between the Gracile Australopithecus Africanus
642   (STS5) and Robust Australopithecus Boisei (OH5), J Vertebr Paleontol 29, 96a-96a.

643   Fitton, L.C., Prôa, M., Rowland, C., Toro-Ibacache, V., O'Higgins, P., 2015. The Impact of
644   Simplifications on the Performance of a Finite Element Model of a *Macaca fascicularis*
645   Cranium, The Anatomical Record 298, 107-121.

646   Fitton, L.C., Shi, J.F., Fagan, M.J., O'Higgins, P., 2012. Masticatory loadings and cranial
647   deformation in *Macaca fascicularis*: a finite element analysis sensitivity study, J Anat 221,
648   55-68.

649   Gans, C., de Vree, F., 1987. Functional bases of fiber length and angulation in muscle,
650   Journal of Morphology 192, 63-85.

651   García-Granero, J.J., Arias-Martorell, J., Madella, M., Lancelotti, C., 2016. Geometric
652   morphometric analysis of Setaria italica (L.) P. Beauv. (foxtail millet) and Brachiaria ramosa
653   (L.) Stapf. (browntop millet) and its implications for understanding the biogeography of small
654   millets, Vegetation History and Archaeobotany 25, 303-310.

655   Godinho, R.M., O'Higgins, P., 2017. Virtual reconstruction of cranial remains: the H.
656   Heidelbergensis, Kabwe 1 fossil, in: Thompson, T., Errickson, D. (Eds.), Human remains -
657   Another dimension: the application of 3D imaging in funerary context, Elsevier, London, pp.
658   135-147.

659   Godinho, R.M., Toro-Ibacache, V., Fitton, L.C., O'Higgins, P., 2017. Finite element analysis
660   of the cranium: Validity, sensitivity and future directions, Cr Palevol 16, 600-612.

661   Groning, F., Fagan, M., O'Higgins, P., 2012. Modeling the Human Mandible Under
662   Masticatory Loads: Which Input Variables are Important?, Anat Rec 295, 853-863.

663   Groning, F., Fagan, M.J., O'Higgins, P., 2011a. The effects of the periodontal ligament on
664   mandibular stiffness: a study combining finite element analysis and geometric
665   morphometrics, J Biomech 44, 1304-1312.

666   Groning, F., Liu, J., Fagan, M.J., O'Higgins, P., 2009. Validating a voxel-based finite element
667   model of a human mandible using digital speckle pattern interferometry, J Biomech 42, 1224-
668   1229.

669   Groning, F., Liu, J., Fagan, M.J., O'Higgins, P., 2011b. Why Do Humans Have Chins?
670   Testing the Mechanical Significance of Modern Human Symphyseal Morphology With Finite
671   Element Analysis, Am J Phys Anthropol 144, 593-606.

672   Gunz, P., Mitteroecker, P., Bookstein, F., Weber, G., 2004. Computer-aided reconstruction of
673   incomplete human crania using statistical and geometrical estimation methods, Computer
674   Applications and Quantitative Methods in Archaeology, Archaeopress, pp. 92–94.

675   Gunz, P., Mitteroecker, P., Neubauer, S., Weber, G.W., Bookstein, F.L., 2009. Principles for
676   the virtual reconstruction of hominin crania, J Hum Evol 57, 48-62.

677   Hein, A., Georgopoulou, V., Nodarou, E., Kilikoglou, V., 2008. Koan amphorae from
678   Halasarna – investigations in a Hellenistic amphora production centre, J Archaeol Sci 35,
679   1049-1061.

680   Holland, M., 2013. The effect of the inclusion of the periodontal ligament upon the stiffness
681   of a human cranial finite element model: a validated sensitivity study, HYMS, University of
682   York, York.

683   Josephson, R.K., 1975. Extensive and intensive factors determining the performance of
684   striated muscle, J Exp Zool 194, 135-153.

685   Kikuchi, M., Korioth, T.W.P., Hannam, A.G., 1997. The Association Among Occlusal
686   Contacts, Clenching Effort, and Bite Force Distribution in Man, J Dent Res 76, 1316-1325.

687   Kilikoglou, V., Vekinis, G., 2002. Failure Prediction and Function Determination of
688   Archaeological Pottery by Finite Element Analysis, J Archaeol Sci 29, 1317-1325.

689   Kupczik, K., Dobson, C.A., Fagan, M.J., Crompton, R.H., Oxnard, C.E., O'Higgins, P., 2007.
690   Assessing mechanical function of the zygomatic region in macaques: validation and
691   sensitivity testing of finite element models, J Anat 210, 41-53.

692   Ledogar, J.A., Smith, A.L., Benazzi, S., Weber, G.W., Spencer, M.A., Carlson, K.B.,
693   McNulty, K.P., Dechow, P.C., Grosse, I.R., Ross, C.F., Richmond, B.G., Wright, B.W.,
694   Wang, Q., Byron, C., Carlson, K.J., de Ruiter, D.J., Berger, L.R., Tamvada, K., Pryor, L.C.,
695   Berthaume, M.A., Strait, D.S., 2016. Mechanical evidence that Australopithecus sediba was
696   limited in its ability to eat hard foods, Nat Commun 7.

697   Levy, R., Dawson, P., 2009. Using finite element methods to analyze ancient architecture: an
698   example from the North American Arctic, J Archaeol Sci 36, 2298-2307.

699   Lieberman, D., 2011. The Evolution of the Human Head, Harvard University Press,
700   Cambridge.

701   McCormack, S.W., Witzel, U., Watson, P.J., Fagan, M.J., Gröning, F., 2014. The
702   Biomechanical Function of Periodontal Ligament Fibres in Orthodontic Tooth Movement,
703   Plos One 9, e102387.

704   Milne, N., O'Higgins, P., 2012. Scaling of form and function in the xenarthran femur: a 100-
705   fold increase in body mass is mitigated by repositioning of the third trochanter, P Roy Soc B-
706   Biol Sci 279, 3449-3456.

25

707   Neeser, R., Ackermann, R.R., Gain, J., 2009. Comparing the accuracy and precision of three

708   techniques used for estimating missing landmarks when reconstructing fossil hominin crania,

709   Am J Phys Anthropol 140, 1-18.

710   O'Connor, C.F., Franciscus, R.G., Holton, N.E., 2005. Bite force production capability and

711   efficiency in neandertals and modern humans, Am J Phys Anthropol 127, 129-151.

712   O'Higgins, P., Cobb, S.N., Fitton, L.C., Groning, F., Phillips, R., Liu, J., Fagan, M.J., 2011.

713   Combining geometric morphometrics and functional simulation: an emerging toolkit for

714   virtual functional analyses, J Anat 218, 3-15.

715   O'Higgins, P., Fitton, L.C., Phillips, R., Shi, J.F., Liu, J., Groning, F., Cobb, S.N., Fagan,

716   M.J., 2012. Virtual Functional Morphology: Novel Approaches to the Study of Craniofacial

717   Form and Function, Evol Biol 39, 521-535.

718   O'Higgins, P., Milne, N., 2013. Applying geometric morphometrics to compare changes in

719   size and shape arising from finite elements analyses, Hystrix, the Italian Journal of

720   Mammalogy 24, 7.

721   Okumura, M., Araujo, A.G.M., 2014. Long-term cultural stability in hunter–gatherers: a case

722   study using traditional and geometric morphometric analysis of lithic stemmed bifacial points

723   from Southern Brazil, J Archaeol Sci 45, 59-71.

724   Oldfield, C.C., McHenry, C.R., Clausen, P.D., Chamoli, U., Parr, W.C.H., Stynder, D.D.,

725   Wroe, S., 2012. Finite element analysis of ursid cranial mechanics and the prediction of

726   feeding behaviour in the extinct giant Agriotherium africanum, J Zool 286, 171-171.

727   Owen, J., Dobney, K., Evin, A., Cucchi, T., Larson, G., Strand Vidarsdottir, U., 2014. The

728   zooarchaeological application of quantifying cranial shape differences in wild boar and

729   domestic pigs (Sus scrofa) using 3D geometric morphometrics, J Archaeol Sci 43, 159-167.

26

730   Paphangkorakit, J., Osborn, J.W., 1997. Effect of Jaw Opening on the Direction and
731   Magnitude of Human Incisal Bite Forces, J Dent Res 76, 561-567.

732   Parr, W.C.H., Chamoli, U., Jones, A., Walsh, W.R., Wroe, S., 2013. Finite element micro-
733   modelling of a human ankle bone reveals the importance of the trabecular network to
734   mechanical performance: New methods for the generation and comparison of 3D models, J
735   Biomech 46, 200-205.

736   Parr, W.C.H., Wroe, S., Chamoli, U., Richards, H.S., McCurry, M.R., Clausen, P.D.,
737   McHenry, C., 2012. Toward integration of geometric morphometrics and computational
738   biomechanics: New methods for 3D virtual reconstruction and quantitative analysis of Finite
739   Element Models, J Theor Biol 301, 1-14.

740   Prôa, M., 2013. Cranial Form Evolution and Functional Adaptations to Diet among
741   Papionins: A Comparative Study combining Quantitative Genetics, Geometric
742   Morphometrics, and Finite Element Analysis, Hull York Medical School, University of York,
743   York.

744   Quinto-Sánchez, M., Adhikari, K., Acuña-Alonzo, V., Cintas, C., Silva de Cerqueira, C.C.,
745   Ramallo, V., Castillo, L., Farrera, A., Jaramillo, C., Arias, W., Fuentes, M., Everardo, P., de
746   Avila, F., Gomez-Valdés, J., Hünemeier, T., Gibbon, S., Gallo, C., Poletti, G., Rosique, J.,
747   Bortolini, M.C., Canizales-Quinteros, S., Rothhammer, F., Bedoya, G., Ruiz-Linares, A.,
748   González-José, R., 2015. Facial asymmetry and genetic ancestry in Latin American admixed
749   populations, Am J Phys Anthropol, n/a-n/a.

750   Rak, Y., 1983. The Australopithecine Face, in: Rak, Y. (Ed.), The Australopithecine Face,
751   Academic Press, p. 1.

752   Rak, Y., 1986. The Neanderthal - a New Look at an Old Face, J Hum Evol 15, 151-164.

753   Rayfield, E.J., 2005. Aspects of comparative cranial mechanics in the theropod dinosaurs
754   Coelophysis, Allosaurus and Tyrannosaurus, Zool J Linn Soc-Lond 144, 309-316.

755 Rayfield, E.J., 2007. Finite element analysis and understanding the biomechanics and
756 evolution of living and fossil organisms, Annu Rev Earth Pl Sc 35, 541-576.

757 Rayfield, E.J., Norman, D.B., Horner, C.C., Horner, J.R., Smith, P.M., Thomason, J.J.,
758 Upchurch, P., 2001. Cranial design and function in a large theropod dinosaur, Nature 409,
759 1033-1037.

760 Reed, D.A., Porro, L.B., Iriarte-Diaz, J., Lemberg, J.B., Holliday, C.M., Anapol, F., Ross,
761 C.F., 2011. The impact of bone and suture material properties on mandibular function in
762 Alligator mississippiensis: testing theoretical phenotypes with finite element analysis, J Anat
763 218, 59-74.

764 Rohlf, F.J., Marcus, L.F., 1993. A revolution in morphometrics, Trends Ecol Evol 8, 129-
765 132.

766 Ros, J., Evin, A., Bouby, L., Ruas, M.-P., 2014. Geometric morphometric analysis of grain
767 shape and the identification of two-rowed barley (Hordeum vulgare subsp. distichum L.) in
768 southern France, J Archaeol Sci 41, 568-575.

769 Ross, C.F., 2005. Finite element analysis in vertebrate biomechanics, Anat Rec Part A 283A,
770 253-258.

771 Schwartz, J.H., Tattersall, I., 2003. The Human Fossil Record - Craniodental Morphology of
772 Genus Homo, Wiley-Liss, USA.

773 Sellers, W.I., Crompton, R.H., 2004. Using sensitivity analysis to validate the predictions of a
774 biomechanical model of bite forces, Ann Anat 186, 89-95.

775 Senck, S., Bookstein, F.L., Benazzi, S., Kastner, J., Weber, G.W., 2015. Virtual
776 Reconstruction of Modern and Fossil Hominoid Crania: Consequences of Reference Sample
777 Choice, The Anatomical Record 298, 827-841.

778   Senck, S., Coquerelle, M., 2015. Morphological Integration and Variation in Facial

779   Orientation in Pongo pygmaeus pygmaeus: A Geometric Morphometric Approach via Partial

780   Least Squares, Int J Primatol 36, 489-512.

781   Shi, J.F., Curtis, N., Fitton, L.C., O'Higgins, P., Fagan, M.J., 2012. Developing a

782   musculoskeletal model of the primate skull: Predicting muscle activations, bite force, and

783   joint reaction forces using multibody dynamics analysis and advanced optimisation methods,

784   J Theor Biol 310, 21-30.

785   Sinn, D.P., DeAssis, E.A., Throckmorton, G.S., 1996. Mandibular excursions and maximum

786   bite forces in patients with temporomandibular joint disorders, J Oral Maxil Surg 54, 671-

787   679.

788   Slice, D.E., 2001. Landmark coordinates aligned by Procrustes analysis do not lie in

789   Kendall's shape space. Systematic biology, 50(1), 141-149.

790   Slice, D.E., Chalk, J., Smith, A.L., Smith, L.C., Wood, S., Berthaume, M., Benazzi, S.,

791   Dzialo, C., Tamvada, K., Ledogar, J.A., 2013. Viewpoints: Diet and dietary adaptations in

792   early hominins: The hard food perspective, Am J Phys Anthropol 151, 339-355.

793   Smith, A.L., Benazzi, S., Ledogar, J.A., Tamvada, K., Pryor Smith, L.C., Weber, G.W.,

794   Spencer, M.A., Dechow, P.C., Grosse, I.R., Ross, C.F., Richmond, B.G., Wright, B.W.,

795   Wang, Q., Byron, C., Slice, D.E., Strait, D.S., 2015a. Biomechanical Implications of

796   Intraspecific Shape Variation in Chimpanzee Crania: Moving Toward an Integration of

797   Geometric Morphometrics and Finite Element Analysis, The Anatomical Record 298, 122-

798   144.

799   Smith, A.L., Benazzi, S., Ledogar, J.A., Tamvada, K., Pryor Smith, L.C., Weber, G.W.,

800   Spencer, M.A., Lucas, P.W., Michael, S., Shekeban, A., Al-Fadhalah, K., Almusallam, A.S.,

801   Dechow, P.C., Grosse, I.R., Ross, C.F., Madden, R.H., Richmond, B.G., Wright, B.W.,

802   Wang, Q., Byron, C., Slice, D.E., Wood, S., Dzialo, C., Berthaume, M.A., van Casteren, A.,

803   Strait, D.S., 2015b. The Feeding Biomechanics and Dietary Ecology of Paranthropus boisei,

804   The Anatomical Record 298, 145-167.

805 Stayton, C.T., 2009. Application of thin-plate-spline transformations to finite element
806 models, or, how to turn a bog turtle into a spotted turtle to analyze both, Evolution 63, 1348-
807 1355.

808 Strait, D.S., Constantino, P., Lucas, P.W., Richmond, B.G., Spencer, M.A., Dechow, P.C.,
809 Ross, C.F., Grosse, I.R., Wright, B.W., Wood, B.A., Weber, G.W., Wang, Q., Byron, C.,

810 Strait, D.S., Grosse, I.R., Dechow, P.C., Smith, A.L., Wang, Q., Weber, G.W., Neubauer, S.,
811 Slice, D.E., Chalk, J., Richmond, B.G., Lucas, P.W., Spencer, M.A., Schrein, C., Wright,
812 B.W., Byfton, C., Ross, C.F., 2010. The Structural Rigidity of the Cranium of
813 Australopithecus africanus: Implications for Diet, Dietary Adaptations, and the Allometry of
814 Feeding Biomechanics, Anat Rec 293, 583-593.

815 Strait, D.S., Richmond, B.G., Spencer, M.A., Ross, C.F., Dechow, P.C., Wood, B.A., 2007.
816 Masticatory biomechanics and its relevance to early hominid phylogeny: An examination of
817 palatal thickness using finite-element analysis, J Hum Evol 52, 585-599.

818 Strait, D.S., Wang, Q., Dechow, P.C., Ross, C.F., Richmond, B.G., Spencer, M.A., Patel,
819 B.A., 2005. Modeling elastic properties in finite element analysis: How much precision is
820 needed to produce an accurate model?, Anat Rec Part A 283A, 275-287.

821 Strait, D.S., Weber, G.W., Neubauer, S., Chalk, J., Richmond, B.G., Lucas, P.W., Spencer,
822 M.A., Schrein, C., Dechow, P.C., Ross, C.F., Grosse, I.R., Wright, B.W., Constantino, P.,
823 Wood, B.A., Lawn, B., Hylander, W.L., Wang, Q., Byron, C., Slice, D.E., Smith, A.L., 2009.
824 The feeding biomechanics and dietary ecology of Australopithecus africanus, P Natl Acad
825 Sci USA 106, 2124-2129.

826 Szwedowski, T.D., Fialkov, J., Whyne, C.M., 2011. Sensitivity analysis of a validated
827 subject-specific finite element model of the human craniofacial skeleton, P I Mech Eng H
828 225, 58-67.

829 Toro-Ibacache, V., Fitton, L.C., Fagan, M.J., O'Higgins, P., 2016. Validity and sensitivity of
830 a human cranial finite element model: implications for comparative studies of biting
831 performance, J Anat 228, 70-84.

832 Toro-Ibacache, V., Zapata MuÑoz, V., O'Higgins, P., 2015. The Predictability from Skull
833 Morphology of Temporalis and Masseter Muscle Cross-Sectional Areas in Humans, The
834 Anatomical Record 298, 1261-1270.

835 Trinkaus, E., 1987. The Neandertal Face - Evolutionary and Functional Perspectives on a
836 Recent Hominid Face, J Hum Evol 16, 429-443.

837 Wang, Q.A., Smith, A.L., Strait, D.S., Wright, B.W., Richmond, B.G., Grosse, I.R., Byron,
838 C.D., Zapata, U., 2010. The Global Impact of Sutures Assessed in a Finite Element Model of
839 a Macaque Cranium, Anat Rec 293, 1477-1491.

840 Weber, G.W., 2015. Virtual Anthropology, Am J Phys Anthropol 156, 22-42.

841 Weber, G.W., Bookstein, F.L., 2011. Virtual Anthropology - A Guide for a New
842 Interdisciplinary Field, Springer-Verlag, Wien.

843 Weijs, W.A., 1980. Biomechanical Models and the Analysis of Form: A Study of the
844 Mammalian Masticatory Apparatus, Am Zool 20, 707-719.

845 Wilczek, J., Monna, F., Barral, P., Burlet, L., Chateau, C., Navarro, N., 2014. Morphometrics
846 of Second Iron Age ceramics – strengths, weaknesses, and comparison with traditional
847 typology, J Archaeol Sci 50, 39-50.

848 Wood, S.A., Strait, D.S., Dumont, E.R., Ross, C.F., Grosse, I.R., 2011. The effects of
849 modeling simplifications on craniofacial finite element models: The alveoli (tooth sockets)
850 and periodontal ligaments, J Biomech 44, 1831-1838.

851 Wroe, S., 2008. Cranial mechanics compared in extinct marsupial and extant African lions

852 using a finite-element approach, J Zool 274, 332-339.

853 Wroe, S., Ferrara, T.L., McHenry, C.R., Curnoe, D., Chamoli, U., 2010. The

854 craniomandibular mechanics of being human, P Roy Soc B-Biol Sci 277, 3579-3586.
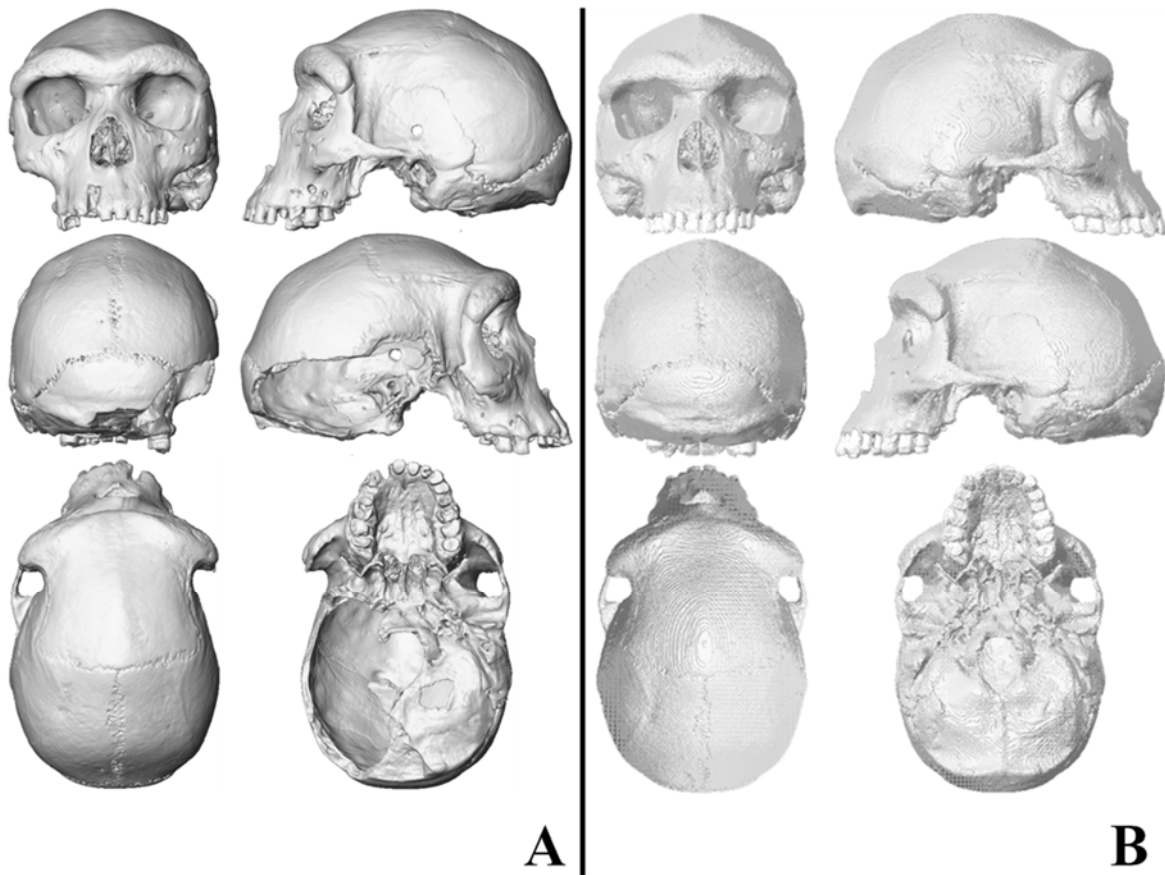

855 Wroe, S., Moreno, K., Clausen, P., Mchenry, C., Curnoe, D., 2007. High-resolution three-

856 dimensional computer simulation of hominid cranial mechanics, Anat Rec 290, 1248-1255.

857 Zollikofer, C.P., Ponce de León, M.S., 2005. Virtual reconstruction: a primer in computer-

858 assisted paleontology and biomedicine, Wiley-Interscience, New Jersey.
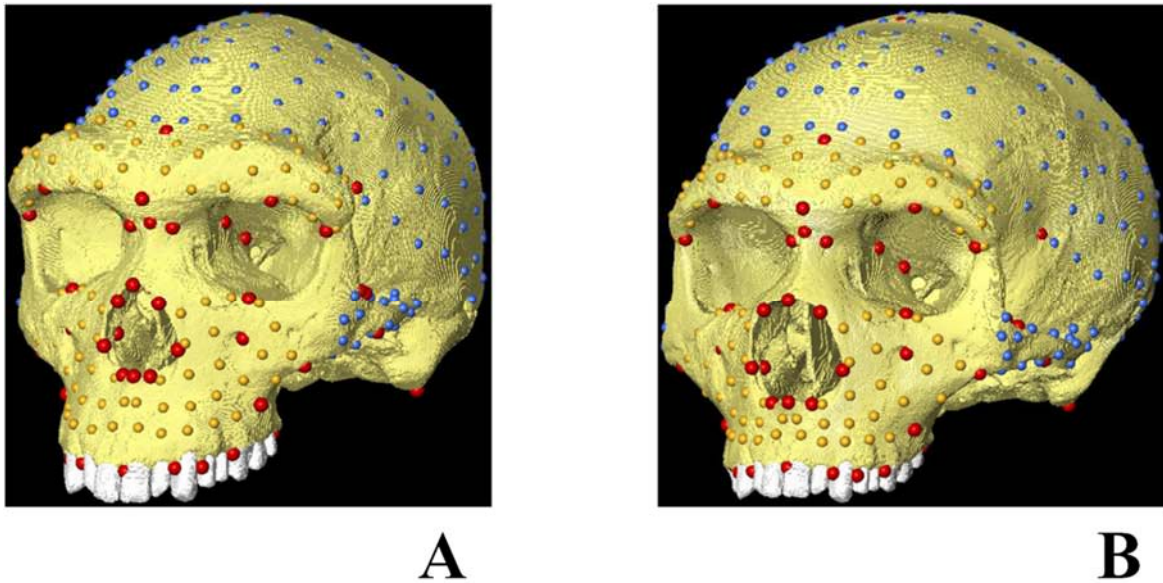
859

860

861

862

Figure 1: Cranium of Kabwe 1 (A) before and (B) after reconstruction.

864

865

868 Figure 2: A reconstructed Kabwe 1, *Homo heidelbergensis* cranium model (A) and a
869 hypothetical *Homo neanderthalensis* (B). The hypothetical Neanderthal was created via
870 surface warping model A into a mean Neanderthal landmark data set (B) using thin plate
871 splines based on classical and sliding semi-landmarks. Conventional landmarks (red spheres);
872 sliding semi-landmarks on the maxilla and brow-ridge (yellow spheres); sliding semi-
873 landmarks of the vault and zygoma (light blue spheres).

874

875
876
877
878
879
880
881
882
883
884
885
886
887
888
889
890

891
892
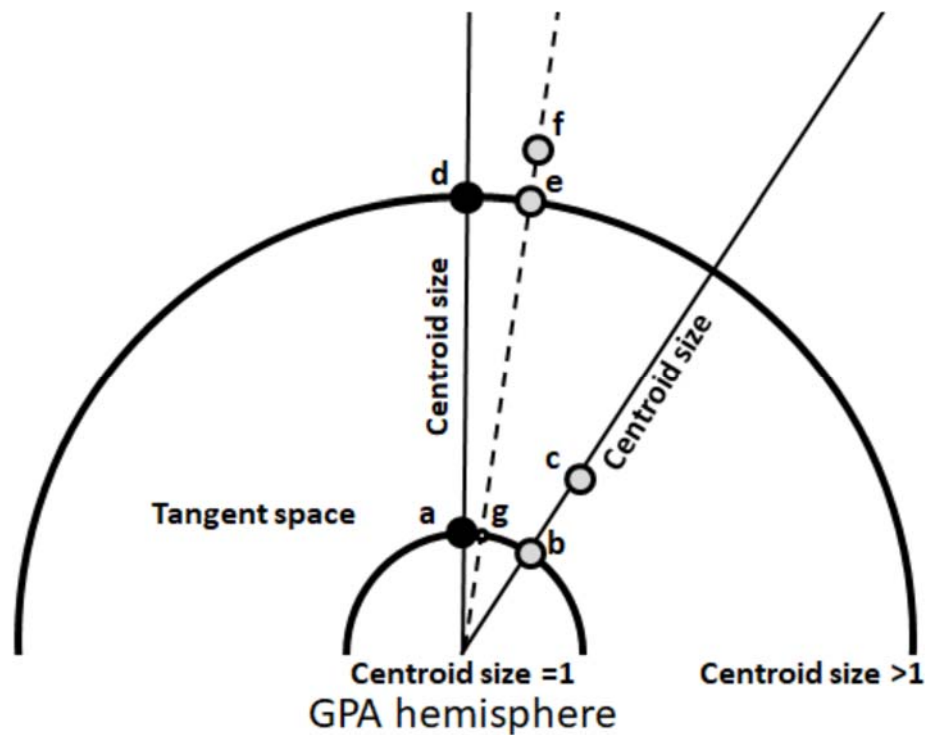893
894
895
896
897
898
899

Figure 3: A schematic illustrating the hemisphere of GPA aligned coordinates (Slice 2001) for triangles, showing the tangent space, the vectors of centroid size, and the size and shape space resulting from rescaling of GPA registered coordinates to centroid size >1. The black points, a and b, represent the same unloaded forms with different centroid sizes. The grey points c and f represent the loaded forms and the grey points b and e represent their projections onto the GPA hemispheres with centroid sizes =1 and >1. G is the projection of f and e onto the GPA hemisphere with centroid size =1. See text for explanation.

900

901

902 Figure 4: PCA of large scale deformations of a sensitivity study assessing the impact of
903 simplifications of material properties in a modern human cranium. Model 1 is not visible
904 because it is in the same location in the plot as model 2. Deformations are magnified by a
905 factor of 500 to facilitate visualisation.

906
907